From Knowledge to Wisdom

Journal of Geological Resource and Engineering

Volume 4, Number 3, March 2016

David Publishing Company
www.davidpublisher.com

ISSN 2328-2193
DOI:10.17265/2328-2193

Journal of Geological Resource and Engineering

Volume 4, Number 3, March 2016 (Serial Number 12)

David Publishing Company
www.davidpublisher.com

Journal of Geological Resource and Engineering 3 (2016) 125-136
doi:10.17265/2328-2193/2016.03.003

Using Statistical Methods for Rock Parameter Identification to Analyse the THM Behaviour of Callovo-Oxfordian Claystone due to Heating

Michael Jobmann[1], Sha Li[1], Mirko Polster[1], Michael Breustedt[1], Roger Schlegel[2], Petr Vymlatil[2] and Johannes Will[2]

1. DBE TECHNOLOGY GmbH, Eschenstrasse 55, Peine D-31224, Germany

2. Dynardo GmbH, Steubenstrasse 25, Weimar 99423, Germany

Abstract: In the framework of a heater experiment at the Meuse/Haute-Marne rock laboratory, DBE TECHNOLOGY and Dynardo performed an analysis of the rock behaviour in response to heating. New approaches describing rock permeability as a function of stress and plastic strain were used, and statistical methods for parameter identification were applied. The methods comprise automatic sensitivity analysis and optimization algorithms that allow a parameter fitting and an analysis of the importance of individual parameters for the general system development. The identification process resulted in a parameter set that allows a good description of the rock behaviour while being heated.

Key words: Claystone, parameter identification, sensitivity analysis, permeability, pore pressure, optimization.

1. Introduction

To study the thermo-hydro-mechanical effects of the thermal transient phase on the clay host rock of a deep repository, ANDRA (the French National Radioactive Waste Management Agency) performs an in-situ heating test called TED experiment. This experiment is the second one carried out in the Meuse/Haute-Marne Underground Research Laboratory focusing on determining the thermo-hydro-mechanical behavior of the Callovo-Oxfordian claystone. The aim of the TED experiment is to measure the temperature, deformation, and pore-pressure field evolution around heaters and to back-analyze the thermo-hydro-mechanical properties of the Callovo-Oxfordian claystone. The TED experiment was also designed to study the evolution of the damaged zone due to heating. The analyses of the TED experiment results will help to calibrate the numerical models that will be applied to the French disposal cell concept [1]. A detailed description of the heater experiment is given in Ref. [2]. One possibility to identify the THM parameters of the claystone is to perform a series of forward simulations by adjusting the THM input parameters until the calculation results fit best to the values measured at the different sensor locations. Given the large number of sensors to consider, and based on experience from former experiments at the Meuse/Haute-Marne and Mont Terri underground research labs [3-5], doing this fitting process manually is a long and laborious task. Thus, an automatic parameter identification process has been applied, and the results are presented in this paper.

Corresponding author: Roger Schlegel, Dr., research fields: CAE-based sensitivity analysis, stochastic analysis, parameter identification, optimization, thermal-hydraulic-mechanical coupled finite element simulation.

2. The Heating Experiment

The test set-up consists of 3 heater boreholes and 21 instrumented observation boreholes. Each heater is 4 m long and generates a thermal power of 1,500 W. The distance between the heaters is 2.6 m in order to approximate the geometry of the planned disposal cells.

The surrounding boreholes were strategically located to take into account the anisotropic THM behavior of the claystone (Fig. 1). There are 12 boreholes for porepressure measurements, 9 boreholes for temperature measurements, and 2 boreholes for deformation measurements. To optimize and simplify the inverse problem analysis, special attention was paid to the reduction of uncertainties regarding the sensors' locations in the boreholes. The incorrect determination of sensor locations in the previous thermal experiment was found to be a very problematic issue for analysis and parameter determination [3].

The central heater was activated on January 25, 2010, starting with a relatively low heating power of 150 W. Subsequently, the heating power was increased to 300 W and finally to 600 W. Each step was about four months long. After one year, the two surrounding heaters were activated, and the same heat load was applied. Before proceeding to the next heating step, permeability tests were performed in all pressure measurement boreholes to investigate the impact of the heat on the permeability of the rock.

3. Methodology for Rock Parameter Identification

The prerequisite for a successful computer simulation is the ability to calculate the main physical phenomena of thermo-hydraulic-mechanical behavior [6] with sufficient accuracy and efficiency. For model calibration corresponding to the experiment, we need a completely parametric model which can be automatically executed to run parameter variations. During calibration, the calculation of several hundred different designs is necessary. Thus, the simulation of one design (one set of possible rock parameter) has to be highly effective. Therefore, the balance between accuracy and efficiency is the challenge when using computer-based simulation for such geotechnical applications.

Dynardo developed a 3D THM simulator by coupling ANSYS parametric modeling and implicit FEM simulation environment with multiPlas [7]. When using a homogenized continuum approach for solving nonlinear geotechnical applications, multiPlas provides adequate geotechnical constitutive material models for

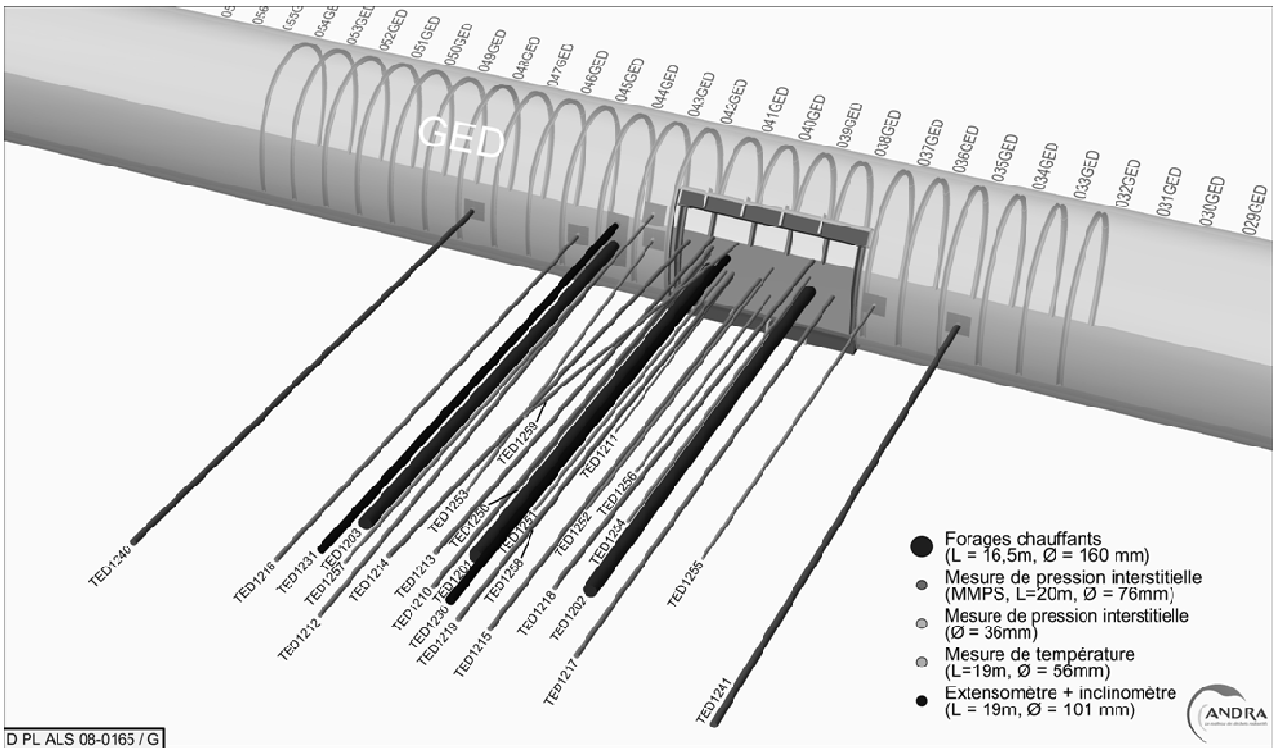

Fig. 1 Location of boreholes in the TED experiment.

ANSYS [8]. To calibrate the numerical model to the in-situ experimental results, the software tool optiSLang [9] was coupled to the THM simulator for CAE-based sensitivity analysis and optimization. The uncertain input parameters for the numerical model from the best in-situ and laboratory data available need to be calibrated to the in-situ measurements.

The model created for the THM analysis of the heating experiment contains the physical phenomena necessary to fit the measurement results. The next challenge is to deal with the uncertainty of the material parameters or the in-situ stress conditions. Even the best in-situ and laboratory test data available contain uncertain parameters or have to be taken from literature. Here, efficient ways of performing sensitivity analyses to identify the most important input parameters and to calibrate the numerical models to experimental data become important. With optiSLang, we perform numerical sensitivity studies for nonlinear problems using optimized stochastic sampling strategies. In Fig. 2 the workflow for parameter calibration is shown.

With Latin Hypercube (LH) sampling, we scan the design space followed by statistical measurements of the importance of individual model parameters using the Coefficient of Determination (CoD). The CoD measures the amount of response parameter variation which results from the input variation of every single uncertain parameter. The basis of this determination measurement is the correlation analysis including linear and nonlinear correlation hypotheses. The detection of nonlinear correlations that have a large number of uncertain parameters with a minimum number of design evaluations is conducted by the Meta-model of Optimal Prognosis (MOP) algorithm. Here, multiple linear and nonlinear correlation models are evaluated in different candidate design spaces of important parameters. Over fitting, as a common problem in large parameter spaces using higher order correlation functions is avoided by the CoD check of the resulting Meta-models at parts of the sample set which are not used to fit the meta-models. In that case, the terminology of the CoD is moved into the Coefficient of Prognosis (CoP), which is the final measurement of the parameter contribution to the variation of important response values. For more details on algorithms we refer to the literature [9-11].

4. Numerical Model

4.1 Model Domain

In view of calculation time, the geometric model size and mesh discretization of the model have to be chosen carefully because dozens of simulations are needed for calibration procedure. At the same time, the boundary conditions have to be placed far enough so they have only insignificant influence on the results. Therefore, different model sizes and discretization levels were tested to find a model that shows the best compromise between accuracy of the results and adequate calculation time.

Good convergence behaviour in the mechanical analysis is achieved by ensuring that the sweep meshing capabilities of ANSYS produce brick only meshes that have controlled element edge length conditions. The total model domain and the mesh are shown in Figs. 3a and 3b. In total, 300,000 elements are used. The model domain contains the tunnel and the niche at the URL with shotcrete surfaces, the three

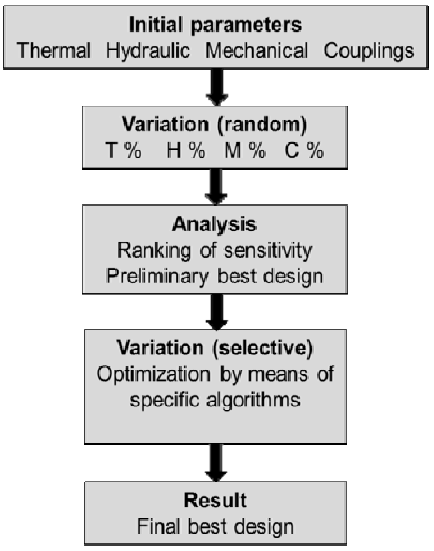

Fig. 2 Work flow of parameter calibration.

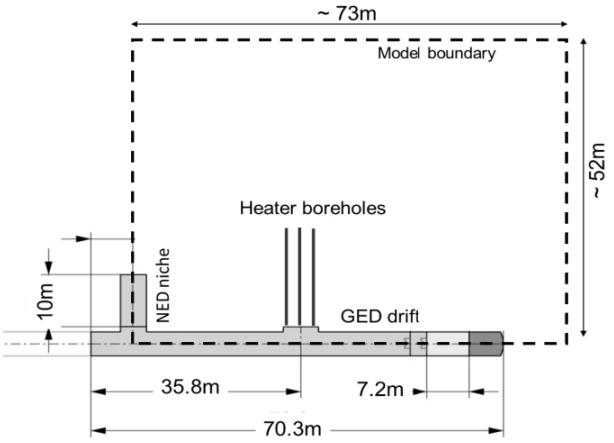

Fig. 3a Model domain.

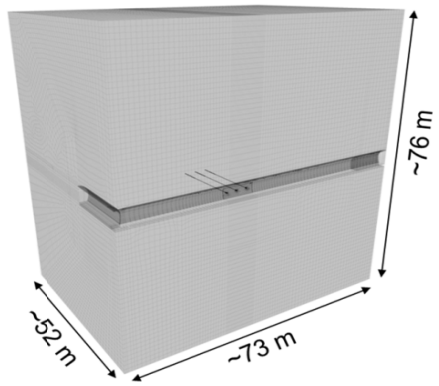

Fig. 3b Numerical mesh.

boreholes with the heaters, and two observation boreholes intended for mechanical deformation measurements. The latter act as hydraulic sinks in the domain and have therefore been considered in the model. For FEM modelling, 8 node solid elements which have temperatures, hydraulic heights, and displacements as degrees of freedoms are used.

4.2 Constitutive Models

The process of the THM coupled simulations is based on the solution of the thermal-hydraulic and nonlinear mechanical analyses using forward coupling at discrete time steps. All analyses are coupled with explicit forward schemata i.e., material parameters, DOFs, and loads in the next step are updated depending on the results of the previous steps.

Fig. 4 shows a schematic view of THM phenomena and coupling. The following important couplings are taken into account: update of pore pressure as a result of temperature change (T→H) including effects on stress strain fields from thermal expansion (T→M); update of hydraulic conductivity depending on the stress state as well as on plastic strain (damage, fracturing) (M→H); update of pore pressure as a result of stress induced deformation (M→H); and update of effective stresses as a result of pore pressure changes (H→M).

The following couplings with second order influence were neglected: degree of water saturation and effect of convection (H→T) and stress strain effects on thermal conductivity (M→T).

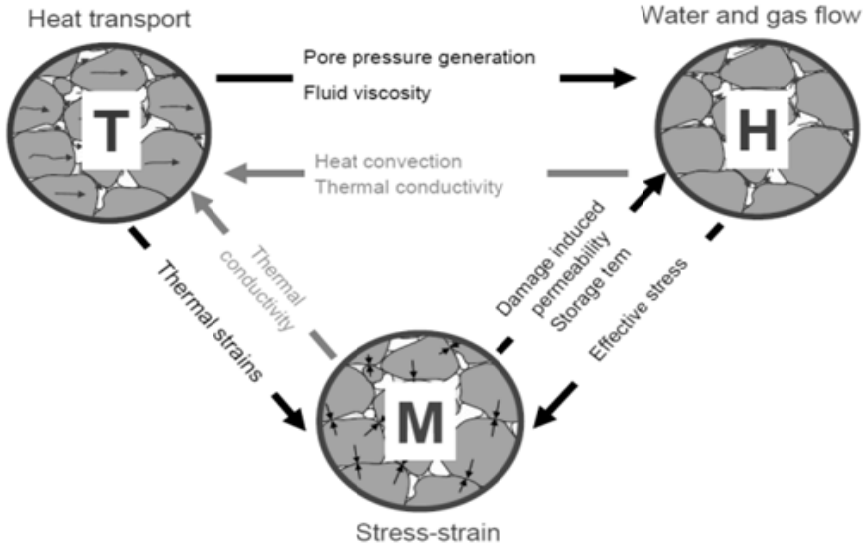

Fig. 4 Main phenomena of THM coupling and their interaction [12].

For solving coupled THM problems, the following balance equations and transport laws are used:

- Equation of motion and equilibrium (mechanical nonlinear analysis);
- Equation of energy balance (thermal analysis);
- Equation of fluid-mass balance (hydraulic analysis);
- Fourier's Law of heat conduction;
- Darcy's Law of fluid flow in a porous medium.

For numerical solution of heat-flow problems, the code uses the equation of energy balance and transport laws, which are derived from Fourier's Law of heat conduction. The energy balance equation can be written in the following differential expression:

$$\text{grad } q^t + q^t_v = \rho c \, dT/dt \qquad (1)$$

where q^t is the heat-flux vector [W/m^2], q^t_v is the volumetric heat-source intensity [W/m^3], ρ is the density [kg/m^3], c is the specific heat at constant volume [J/kg·K], T is the temperature [°C] and t is the time [s]. Transport of heat is taken into account by heat conduction. The dependence between heat flux and temperature gradient (Fourier's Law) for anisotropic case can be written in the following form:

$$q^t = -\lambda \text{ grad } T \qquad (2)$$

where λ is the thermal conductivity tensor [W/m·K]. The forward coupling to the mechanical stress calculation is carried out via the thermal expansion coefficient α_s. Thermal-strain increments ε^T associated with the free expansion corresponding to temperature change ΔT:

$$\Delta\varepsilon^T = \alpha_s \Delta T \delta \qquad (3)$$

where α_s is the coefficient of linear thermal expansion [1/K], ΔT is the temperature difference [K], and δ the Kronecker delta. For numerical solution of fluid-flow problems, the equation of fluid-mass balance and Darcy's law of fluid transport in a porous medium are used. The fluid-mass balance equation can be given in the following form:

$$\text{grad } q^f + q^f_v = d\zeta/dt \qquad (4)$$

where q^f is the specific discharge vector [1/s], q^f_v is the volumetric fluid source intensity [1/s], ζ is the variation of fluid volume per unit volume of porous material due to diffusive fluid mass transport, and t is time [s]. The relation between the specific discharge vector and the pore pressure is defined by Darcy's law. For the anisotropic case it can be given in the form:

$$q^f = -k/\mu(T) \; grad(P_p - \rho_f g \, z) \text{ or } q^f = -k \; \rho_f \, g/\mu(T) \; grad(h) \qquad (5)$$

where k is the permeability tensor [m^2], $\mu(T)$ is the temperature-dependent fluid viscosity [Pa·s], P_p is the pore pressure, ρ_f is the fluid density [kg/m^3], g is the gravity acceleration [m·s^{-2}], and $h=P_p/g\rho_f + z$ is the hydraulic head [m]. Single-phase flow is considered in the simulation. The anisotropic permeability tensor depends on the stress state as well as on the plastic strain.

$$k_i = k_{\sigma,i} + k_{\varepsilon,i} \text{ for } i=x, y, z \qquad (6)$$

An exponential relation between intrinsic permeability and stress state is introduced for permeability parallel to bedding plane $k_{\sigma,x} = k_{\sigma,y}$ and perpendicular to bedding plane $k_{\sigma,z}$ as follows:

$$k_{\sigma,x} = k_{\sigma,y} = k_{0,p} \times \left(\frac{\sigma_z}{\sigma_0} \right)^{-n_p}$$

$$k_{\sigma,z} = k_{\sigma,n} = k_{0,n} \times \left(\frac{\sigma_{m,h}}{\sigma_0} \right)^{-n_n} \qquad (7)$$

where σ_0= 1 MPa, $k_{0,p}$,n_p, $k_{0,n}$, n_n are parameters, σ_z is vertical stress vertical stress and $\sigma_{m,h}=(\sigma_x+\sigma_y)/2$ is the mean value of horizontal stresses. Permeability change caused by plasticity is considered as linearly dependent on the sum of plastic strains in the plane perpendicular to the considered direction:

$$\begin{aligned} k_{\varepsilon,x} &= k_\varepsilon (\varepsilon_y^+ + \varepsilon_z^+), \; k_{\varepsilon,x} \le k_{\varepsilon,max} \\ k_{\varepsilon,y} &= k_\varepsilon (\varepsilon_x^+ + \varepsilon_z^+), \; k_{\varepsilon,y} \le k_{\varepsilon,max} \\ k_{\varepsilon,z} &= k_\varepsilon (\varepsilon_x^+ + \varepsilon_y^+), \; k_{\varepsilon,z} \le k_{\varepsilon,max} \end{aligned} \qquad (8)$$

where ε_x^+, ε_y^+, ε_z^+ are plastic strains in directions x, y, z; k_ε is the permeability, and $k_{\varepsilon,max}$ is the maximum permeability. Changes in the variation of pore pressure P_p are related linearly to changes in fluid content ξ, volumetric strain ε_v and temperature T by the following constitutive law:

$$\frac{1}{M}\frac{\partial P}{\partial t} = \frac{\partial \zeta}{\partial t} - \alpha \frac{\partial \varepsilon_v}{\partial t} + \beta \frac{\partial T}{\partial t} \qquad (9)$$

where M is the Biot modulus [Pa], α is the Biot coefficient [-], and β the undrained thermal coefficient [1/K] defined as:

$$\beta = 3\,[\alpha_s\,(\alpha - n) + \alpha_{f,\,fact}\,\alpha_f\,(T)\,n] \qquad (10)$$

where α_s is the linear thermal expansion coefficient for grains [1/K], $\alpha_f(T)$ is the temperature-dependent linear thermal expansion coefficient for fluid [1/K], n is the porosity, and $\alpha_{f,\,fact}$ is the factor of $\alpha_f(T)$, which was introduced as a parameter for sensitivity analysis and calibration that simply allows to consider different types of pore fluids.

Due to the bedding of the Callovo-Oxfordian clay, it is very important to take into account the anisotropy of elastic mechanical behaviour and hydraulic conductivity behaviour in the modelling. In addition, with multiPlas [7], we defined a Mohr-Coulomb based elasto-plastic behaviour for the rock matrix as well as for the bedding plane. The behaviour considers shear and tensile failure including softening after the initial strength values are violated. The definition of four yield surfaces results in a multi-surface plasticity definition that is not easy to formulate consistently using implicit FEM codes. One of the main advantages of multiPlas [7] is the automatic procedure to ensure consistent numerical treatment of multi-surface plasticity to achieve convergence behaviour as best as possible.

4.3 Initial and Boundary Conditions

When calibrating complex non-linear time-depended problems, the model initialization is very important. We covered the impacts of tunnel excavation and heater placement on the temperature and pore pressure fields by explicitly modelling excavation and heater placement. The whole model domain is initialized at starting time (t = -605 days) with a constant temperature of 21.5 °C, constant hydraulic height (438.33 m), and initial anisotropic total stress. The boundary conditions for thermal and hydraulic analysis were defined at the model surfaces as fixed or perfectly insulated. For the mechanical analysis, zero displacements were applied normal to the surface at the sides as well as at the lower boundary of the model. The upper boundary was loaded with a pressure that represents the weight of the upper layers.

Later on, the boundary conditions were adjusted during the excavating and drilling of boreholes by introducing new boundary conditions on free surfaces of excavation caverns and boreholes (measured tunnel temperature and zero pore pressure on free surfaces). The tunnel and niche excavation was done in 115 steps (time -604 ... -234.5 days) by deactivating and activating tunnel and lining elements. The same procedure was used to simulate the drilling of the three heater boreholes where clay was deactivated and heater elements activated at the installation times of the heaters. We also took into account the influence of the two observation boreholes next to the heater boreholes. On their longitudinal axes, zero pore pressure was set from the time of drilling.

5. Simulation of the Heater Test

5.1 Temperature Evolution

The basic THM simulation carefully modeled the experiment including the tunnel excavation, the heater boreholes, and all heating phases. The thermal analysis does not depend much on hydraulic or mechanical processes but is the driving force for all the hydro-mechanical processes in the experimental area. Therefore, the thermal rock material properties were calibrated separately at the beginning to ensure a good representation of the temperature evolution in the model.

In Fig. 5, the location of the temperature sensors is shown as a top view onto the horizontal x-y-plane. The sensors are located in eight observation boreholes at different distances to the test drift. The three thick lines represent the locations of the heaters. The initial input parameters as starting values for the parameter identification were taken from laboratory investigations

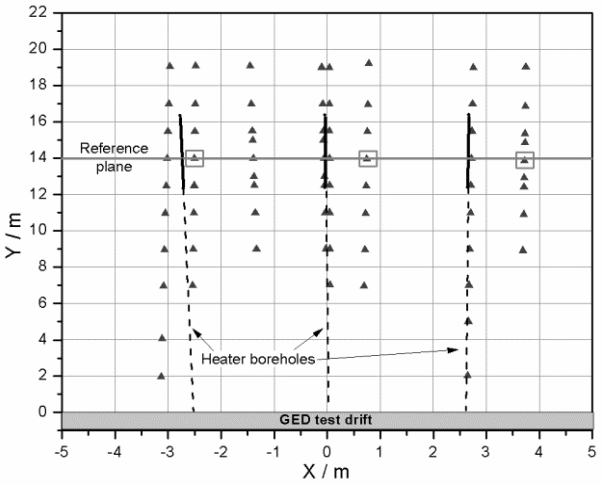

Fig. 5 Location of temperature sensors and heaters (top view).

Table 1 Initial and final thermal properties.

Input parameter		Initial values	Final values
Density	ρ (kg × m^{-3})	2,378	2,333
Horizontal thermal conductivity	λx (W × m^{-1} × K^{-1})	2.00	2.02
Vertical thermal conductivity	λz (W × m^{-1} × K^{-1})	1.31	1.37
Specific heat capacity	c (J × kg^{-1} × K^{-1})	828	695

on drill core samples and are given in Table 1 [13].

For comparison, the best design parameter set found after 40 simulation runs controlled by optiSLang is given in Table 1 as well. It shows that the final values are quite close to the initial ones found in the laboratory. Fig. 6a shows a comparison of the measured and calculated temperature evolutions for three selected sensors. The locations of these sensors are marked in Fig. 5 with a square. The good fitting is evident.

In Fig. 6b the differences between measured and calculated values are given for the eight sensors located at a distance of 14 m from the test drift (reference plane, grey line in Fig. 5). The differences are less than 0.8 K. This is a sound basis for the following identification of the pore water pressure evolution in the experimental area.

5.2 Porewater Pressure Evolution

After the boundary conditions had been adjusted with the help of the initial best guesses for all rock

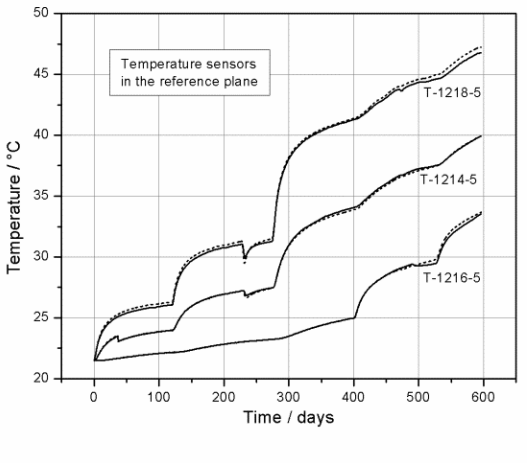

(a)

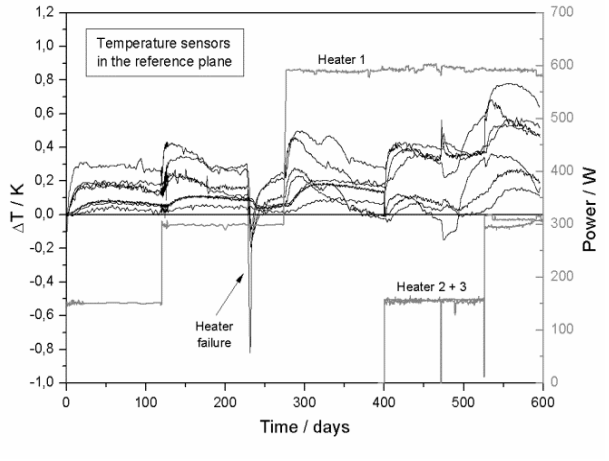

(b)

Fig. 6(a) Comparison of measured and calculated temperature evolutions for three selected sensors, (b) differences between measured and calculated values given for the eight sensors located in the reference plane at a distance of 14 m from the test drift (grey line in Fig. 5).

parameters, the design showed plausible results. This design, together with windows of uncertainty of ± 20%, was used to perform a sensitivity analysis. The input parameters are listed in Tables 2 and 3 (29 uncertain parameters in total). For the sensitivity analysis, 80 designs were generated using optiSLang's Latin Hypercube sampling. The responses of the sensitivity analysis are integral and discrete values of pore pressures obtained from time history signals at all measured points. From each signal, total values of pore pressure were used at time 0 and relative values (related to time 0) at times 20, 121, 141, 275, 295, 400, 420, 526, 546 and 597 days (responses are shown in Fig. 7).

Table 2 Hydraulic and coupling input parameters.

Input parameter		Value
Constants of permeability functions	$k_{0,p}$(m^2)	6.00E-19
	n_p(-)	0.80
	$k_{0,n}$(m^2)	1.50E-20
	n_n(-)	0.2
	k_ε(m^2)	1.00E-14
	$k_{\varepsilon,max}$(m^2)	1.00E-16
Scaling factor of thermal expansion function (pore water)	$\alpha_{f,factor}$ (-)	0.50
Porosity	n(-)	0.17
Thermal expansion coefficient (intact)	α_s (°C^{-1})	1.30E-05
Biot modulus	M (Pa)	4.90E+09
Biot coefficient	α (-)	0.6

Table 3 Mechanical input parameters.

Input parameter		Value
Elasticity constants (transversal Isotropic)	E_p (Pa)	8.230E+09
	E_n (Pa)	5.731E+09
	ν_p (-)	0.3
	ν_{np} (-)	0.3
	G_{np} (Pa)	2.70E+09
Friction angle (intact)	φ_g (°)	25.0
Dilation angle (intact)	ψ_g (°)	10.0
Cohesion (intact)	c_g (Pa)	4.50E+06
Tensile strength (intact)	σ_t (Pa)	1.30E+06
Residual strength values defined as coefficients to initial strength values	$\varphi_{gr,fact}$ (-)	0.70
	$c_{gr,fact}$ (-)	0.40
	$\sigma_{tr,fact}$ (-)	0.40
Friction angle (bedding plane)	φ_1 (°)	20
Cohesion (bedding plane)	c_1 (Pa)	1.50E+06
Tensile strength (bedding plane)	σ_{t1} (Pa)	5.00E+05
Ratios of residual to initial strength factors (bedding plane)	$\varphi_{r1,fact}$ (-)	0.70
	$c_{r1,fact}$ (-)	0.40
	$\sigma_{tr1,fact}$ (-)	0.40

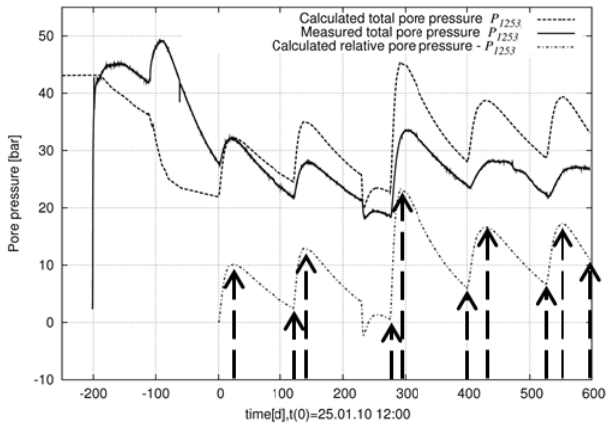

Fig. 7 Pore pressures in borehole TED 1253 for different times.

These time points represent the beginnings and the ends of the heating phases and the times when the maximum values during a heating phase occur.

The important results of the sensitivity analysis are CoP values (Coefficient of Prognosis) which show the significance of input parameters. The CoP results are summarized in Table 4 for absolute pore pressures at the beginning of the heating experiment (time 0) and two relative pore pressures (at time 295 days and 400 days). The CoPs of the responses (total values) are very high, most of them over 90%. This proves the automatic variable reduction and Meta-model generation process of optiSLang using 80 design points only in 29 dimensions. The CoPs of individual input parameter influences on every response variation are colored in accordance with their contribution between 5 and 60%. Zero means the optiSLang internal parameter reduction process has eliminated the input parameter from the meta-model that approximated the response variation. Due to statistical errors that occur when using only 80 designs in up to 29 dimensions, all CoPs below 5% are not trustworthy. We concentrated on influences with a contribution of more than 5%. The CoPs at the beginning of heating (time 0) indicate that during tunnel excavation and borehole drilling for the measurement points 1,251, 1,252, 1,253 and 1,255, which are located in the so-called "reference plane" at a depth of 14 m, the most important parameters are $k_{0,p}$ and n_p (see Eq. 7). For measurement points 1,258 and 1,259, which are located out of the reference plane, the most important parameter is $k_{0,n}$ (7). At some points, especially 1,251, which is very close to the middle heater, the important influence of the strength parameters φ_g, c_g (effect of plasticity) can be seen. The CoPs at time 295 and 400 days identify the important input parameters regarding the maximum pore pressure during the 3rd heating phase and the end value of the 3rd heating phase. Here, the factor of the thermal expansion function (pore water expansion) $\alpha_{f,factor}$, the porosity n, and the Biot modulus M are very important as well.

Table 4 CoPs of the pore pressure values at different times.

	E_p	E_m	ν_p	ν_{mp}	G_{mp}	φ_g	ψ_g	c_g	σ_t	$\varphi_{gr,fact}$	$c_{gr,fact}$	$\sigma_{t,fact}$	φ_1	c_1	σ_{t1}	$\varphi_{1,fact}$	$c_{1,fact}$	$\sigma_{t1,fact}$	$k_{0,p}$	n_p	$k_{0,n}$	n_n	k_ε	$k_{\varepsilon,max}$	$\alpha_{f,factor}$	n	α_g	M	α	Total	
AbsPress1251_0					1%	14%		28%		3%	4%		2%	1%			1%		4%	18%			4%					11%		92%	1251
RelaPress1251_295		1%				16%		23%		5%	6%								1%	10%			2%		9%	9%		4%	1%	86%	
RelaPress1251_400	5%			2%		29%		18%		9%	10%									3%				3%		1%		3%		82%	
AbsPress1252_0						5%		9%		1%	2%								15%	54%	2%		1%					8%		96%	1252
RelaPress1252_295						2%		4%			1%								1%	6%					32%	28%	1%	18%	1%	95%	
RelaPress1252_400		1%				4%		7%		1%	3%			0%					4%	25%			2%		23%	20%	1%	4%	2%	94%	
AbsPress1253_0						6%		13%		1%	2%		1%						12%	45%	1%		2%					11%		94%	1253
RelaPress1253_295						4%		10%		2%	3%								2%	12%					27%	23%		13%	2%	95%	
RelaPress1253_400		1%				11%		15%		5%	8%								2%	28%			2%		12%	12%		2%		94%	
AbsPress1255_0						4%		8%			1%								18%	56%	2%		1%					7%		96%	1255
RelaPress1255_295		2%				4%	1%	13%		1%	5%			1%						2%			4%		22%	20%	1%	13%		90%	
RelaPress1255_400		1%				4%		10%		1%	4%			1%					2%	7%			3%		26%	22%	1%	13%		93%	
AbsPress1258_0		1%						1%													49%	7%			2%	1%		33%	2%	97%	1258
RelaPress1258_275						3%		8%			1%								1%	4%	8%	2%	1%		34%	26%	1%	5%	2%	96%	
RelaPress1258_295								3%											1%	4%	1%				37%	29%	1%	19%	2%	96%	
AbsPress1259_0																				1%	52%	8%			6%	3%		24%	3%	96%	1259
RelaPress1259_295																			2%	3%	6%				39%	29%	2%	12%	4%	96%	
RelaPress1259_400						2%		4%											2%	7%	7%	2%			35%	28%	1%	6%	3%	95%	

CoP = 0%
0% < CoP < 5%
5% ≤ CoP < 10%
10% ≤ CoP < 20%
20% ≤ CoP < 40%
40% ≤ CoP < 60%
60% ≤ CoP < 80%

Table 5 Best design parameter set.

Input parameter		best Design
Friction angle (intact)	φ_g (°)	28.79
Cohesion (intact)	c_g (MPa)	3.794
Ratios of residual to initial strength factors (intact)	$\varphi_{gr,fact}$ (-)	0.84
	$c_{gr,fact}$ (-)	0.444
Friction angle (bedding plane)	φ_1 (°)	23.54
Constants of permeability functions	$k_{0,p}$ (m^2)	5.87E-19
	n_p (-)	1.07871
	$k_{0,n}$ (m^2)	1.50E-20
	n_n (-)	0.15363
	k_ε (m^2)	9.92E-15
	$k_{\varepsilon,max}$ (m^2)	1.18E-16
Scaling factor of thermal expansion function (pore water)	$\alpha_{f,factor}$ (-)	0.344
Porosity	N (-)	0.1646
Biot modulus	M (GPa)	3.9
Biot coefficient	α (-)	0.65

For the next calibration step using optimization algorithms, only input parameters with COPs > 5% were identified. Thus, the final reduced variable space has 15 uncertain parameters (see Table 5). It should be noted that the reduction to parameters showing significant sensitivity to response values, which are used in the objective function, is very important. For insensitive parameters any optimizer would choose only arbitrary values because they will not have significant influence on the objective function.

After parameter reduction, the next challenge was the formulation of an appropriate suitable objective function. Here, we used the sensitivity study again to test different approaches, like Euclidian distance, values at single time steps, or relative values between time steps to compare the measurements with the simulation results to exclude initialization discrepancies. By evaluating the CoP values, we can measure the unexplainable amount of variation (100%-CoP) at every response value. Unexplainable variation results from extraction or approximation noise or from multiple mechanisms influencing the result. Especially integral values may end up with low CoPs. But low CoPs mean that any optimizer will see a lot of noise at the values and will have difficulty calibrating. Therefore, only response values having high CoPs should be used in the formulation of the objective function. In our case, the relative integral values for specific time windows showed reasonable CoPs and were used in the objective function to calibrate the calculated time signals with the measured signals:

$$\Phi = 0.6 \times \sum_i \Phi_{i,I} + 0.8 \times \sum_i \Phi_{i,II} + \sum_i \Phi_{i,III} \quad (11)$$

where $\Phi_{i,I}$ is the integral difference between the calculated and measured relative signals for the 1st heating phase, $\Phi_{i,II}$ for the 2nd heating phase, and $\Phi_{i,III}$ for the 3rd, 4th, and 5th heating phases at measure point i. The meaning of relative integral values is shown in

Fig. 8. This approach was chosen because the numerical simulation cannot reproduce all effects of the initial pore pressure field at the beginning of the heating experiment.

This is most likely due to the drilling of boreholes for measuring equipment installation that cannot be considered in the simulation. To exclude these initial discrepancies from the calibration process, we introduced relative difference functions. We also used the information for weighting factors at the objective function. The initial discrepancies highly influence the first and second heating phase. Therefore, the first and second term in the objective function have lower weighting factors (0.6 and 0.8 respectively).

For solving the calibration problem of minimizing the difference between simulation and measurement, two optimization algorithms were used. Starting from the best design of the sensitivity analysis, we used optiSLang's adaptive response surface method. This methodology follows the main trends to improve the fitting. In a second step, we used evolutionary algorithms for further local refinement of parameter values. The best design parameters are listed in Table 5 (not listed parameters have to be taken from Tables 2 and 3 to complete the input data set).

Fig. 9 compares the results of the best design after calibration with the measurements at two selected boreholes. Borehole TED1252 (left) is located between two heaters and TED1259 is located below the middle heater. The pore pressures fit quite well at these two locations and represent a good fitting quality for horizontal and vertical flow. For most of the measurement points, a good fit could be achieved. For some points, we could not fit the initial condition perfectly, but the gradients and shapes at the heating periods fit well. This proves that the most important physical phenomena of the THM coupling are implemented appropriately in the simulation, and the calibration process to identify the most important rock parameter values is successful.

6. Evaluation and Conclusions

Using ANSYS and multiPlas, a 3-dimensional parametric THM simulator was set up that could be calibrated to in-situ measurement results of a heater experiment. A high numerical efficiency of the simulator was achieved. The simulator needed 32 hours to calculate one design of the calibration process running in-situ stress generation and three heating periods with an up-to-date dual core workstation in 2011.

OptiSLang's functionality for sensitivity analysis and calibration dealing with a large amount of uncertainties was linked to the simulator and, with a correlation analysis the main rock parameters were identified, making visible the mechanism of how the rock parameter variation effects important THM simulation results. This knowledge is essential for defining appropriate boundary conditions for the calibration, appropriate parameter space, constraints, and an objective function. Depending on the number of important parameters that can be calibrated and on the non-linearity of the calibration results, we chose between gradient-based, adaptive response surface-based, or natural inspired optimization algorithms as well as a mix of them.

Based on well determined laboratory data of the thermal rock properties, which were used as input data and for determining the uncertainty range, a good fit

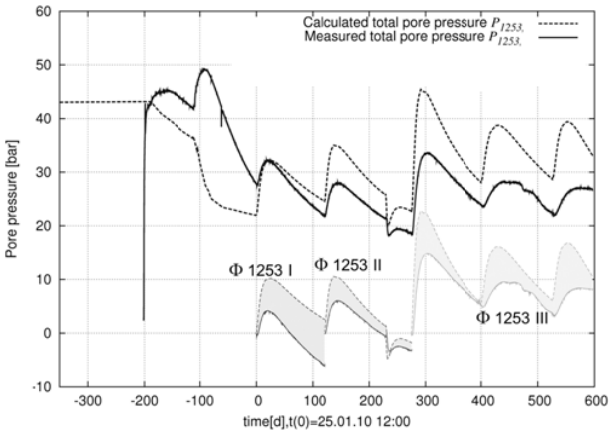

Fig. 8 Integral differences for objective function at TED 1253.

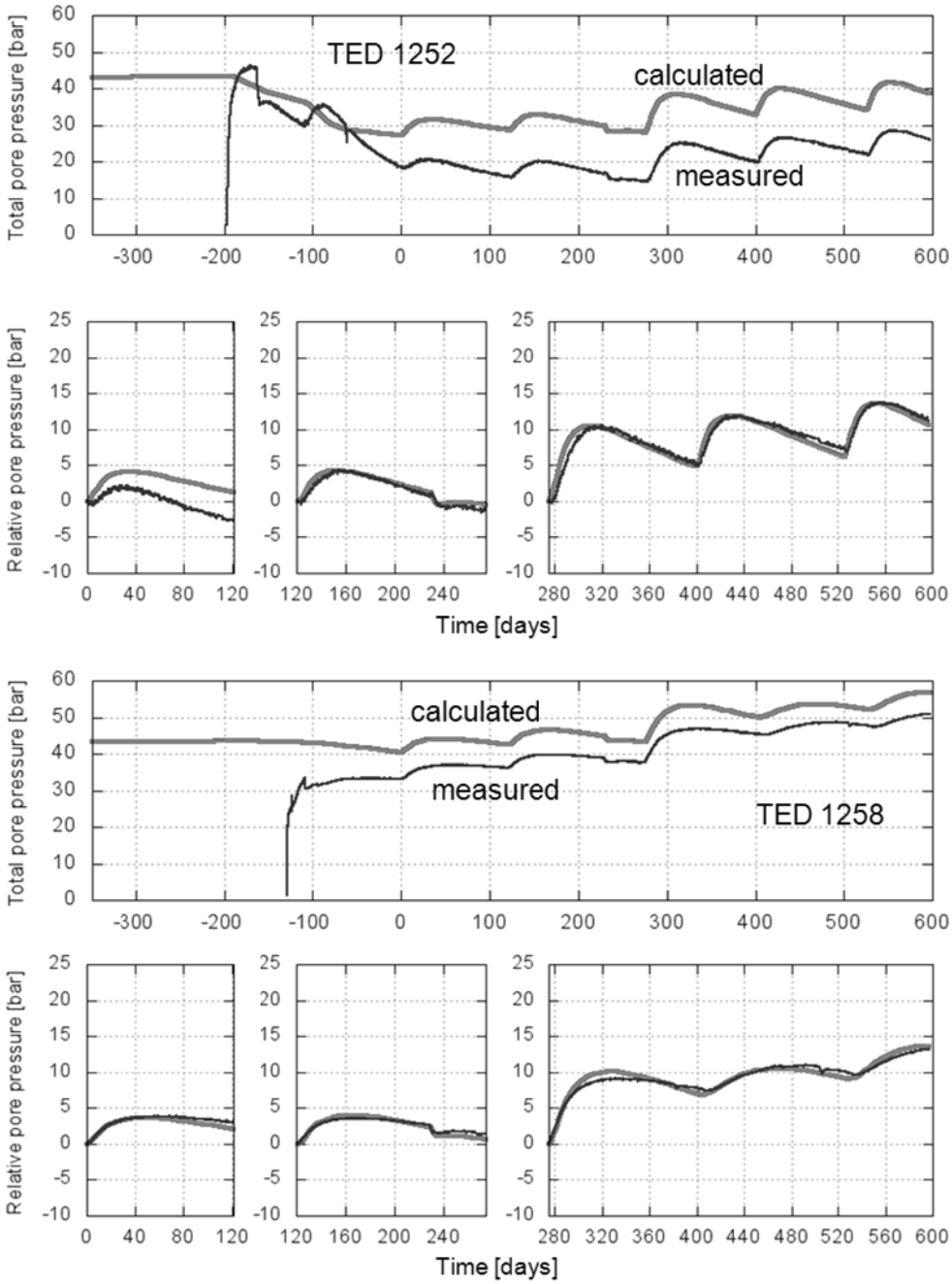

Fig. 9 Comparison of best design with measured pore pressures versus time (absolute and relative) at two locations (TED 1252 and TED 1258).

between measurement results and the simulation of the temperature evolution around the heaters could be achieved and, thus, the identification of the thermal in-situ rock properties was successful. Taking the correct simulated temperature evolution as a sound basis for calculating the pore water pressure evolution, a good fit between measurement and simulation results during the heating phases could be achieved as well. The newly implemented constitutive laws that describe the permeability as functions of anisotropic stress and plastic strain have proven their suitability. In general, a material model is available that allows the description of the THM rock behaviour in response to heating for temperatures ≤ 100 °C.

Acknowledgements

We would like to thank the Federal Ministry of Economics and Energy (BMWi = Bundesministerium für Wirtschaft und Energie) for funding the research and development activities described in this paper under contract No. FKZ 02E10210.

References

[1] ANDRA. 2005. *Andra Research on the Geological Disposal of High-level Long-lived Radioactive Waste—Dossier 2005—Results and Perspectives.* ANDRA, Châtenay-Malabry, France.

[2] Conil, N., Armand, G., Garitte, B., Jobmann, M., Jellouli, M., Fillipi, M., De La Vaissière, R., and Morel, J. 2012. "In-situ Heating Test in the Callovo Oxfordian Clay: Measurement and Interpretation." *Clays in Natural and Engineered Barriers for Radioactive Waste Confinement, 5th International Meeting*, Montpellier, France.

[3] Garitte, B., Vaunat, J., Gens, A., and Armand, G. 2010. "3D Interpretation of an in-situ Heating Test in the Callovo-Oxfordian Mudstone." *Clays in Natural & Engineered Barriers for Radioactive Waste Confinement,* Nantes, France, 29th March-1st April 2010.

[4] Jobmann, M., and Polster, M. 2007. "The Response of Opalinus clay due to Heating—A Combined Analysis of In-situ Measurements, Laboratory Investigations and Numerical Calculations." *Clay in Natural and Engineered Barriers for Radioactive Waste Confinement, Conference Proceedings,* Tours, France.

[5] Wileveau, Y., Su, K., and Ghoreychi, M. 2007. "A Heating Experiment in the Argillites in the Meuse/Haute-Marne Underground Research Laboratory." *11th International Conference on Environmental Remediation and Radioactive Waste Management (ICEM2007)*, September 2-6, 2007, Bruges, Belgium.

[6] Gens, A., Vaunat, B., Garitte, B., and Wileveau, Y. 2007. "In-situ Behavior of a stiff Layered Clay Subject to Thermal Loading: Observations and Interpretation." *Geotechnique* 57 (2): 207-28.

[7] multiPlas. 2010. "Elastoplastic Material Models for ANSYS, Version 6.0. multiPlas User's Manual." Dynardo Gmbh, Weimar. http://www.dynardo.de.

[8] Will, J. 1999. "Dissertation Beitrag zur Standsicherheitsberechnung im geklüfteten Fels in der Kontinuums- und Diskontinuumsmechanik unter Verwendung impliziter und expliziter Berechnungsstrategien, Berichte des Institutes für Strukturmechanik 2/99." Bauhaus Universität Weimar.

[9] optiSLang. 2010. "The Optimizing Structural Language Version 3.1.4, optiSLang Documentation. Dynardo GmbH, Weimar. http://www.dynardo.de.

[10] Will, J. 2006. "The Calibration of Measurement and Simulation as Optimization Problem." In *Proceeding NAFEMS Seminar Virtual Testing—Simulations verfahren als integrierter Baustein einer effizienten Produktentwicklung,* Wiesbaden, Germany.

[11] Most, T., and Will, J. 2010. "Recent Advances in Metamodels of Optimized Prognosis (MoP)." In *Proceedings Weimarer Optimierungs-und Stochastiktage 7.0,* Weimar, Germany.

[12] Gens, A., Vaunat, J., Garitte, B., and Wileveau, Y. 2006. "Response of a Saturated Mudstone under Excavation and Thermal Loading." In *Proceedings of Eurock 2006, Multiphysics Coupling and Long Term Behaviour in Rock Mechanics,* 35-44, Liège, Belgium.

[13] Jobmann, M. 2010. *Thermophysical Properties of Drill Core Samples Taken from TED Experimental Area,* Technical Report, Peine, Germany.

Journal of Geological Resource and Engineering
Volume 4, Number 3, March 2016
David Publishing Company
616 Corporate Way, Suite 2-4876, Valley Cottage, NY 10989, USA
Tel: 1-323-984-7526, 323-410-1082; Fax: 1-323-984-7374, 323-908-0457
http://www.davidpublisher.com, www.davidpublisher.org
geology@davidpublishing.com, geology_davidpublishing@hotmail.com

ISSN 2328-2193
03
9 772328 219167